**Atmospheric
Chemistry
and Physics**

The impact of temperature changes on summer time ozone and its precursors in the Eastern Mediterranean

U. Im[1], K. Markakis[2], A. Poupkou[2], D. Melas[2], A. Unal[3], E. Gerasopoulos[4], N. Daskalakis[1], T. Kindap[3], and M. Kanakidou[1]

[1]Environmental Chemical Processes Laboratory (ECPL), Department of Chemistry, University of Crete, Heraklion, Greece
[2]Aristotle University of Thessaloniki, Department of Physics, Laboratory of Atmospheric Physics, Thessaloniki, Greece
[3]Istanbul Technical University, Eurasia Institute of Earth Sciences, Istanbul, Turkey
[4]Institute for Environmental Research and Sustainable Development, National Observatory of Athens, Athens, Greece

Abstract. Changes in temperature due to variability in meteorology and climate change are expected to significantly impact atmospheric composition. The Mediterranean is a climate sensitive region and includes megacities like Istanbul and large urban agglomerations such as Athens. The effect of temperature changes on gaseous air pollutant levels and the atmospheric processes that are controlling them in the Eastern Mediterranean are here investigated. The WRF/CMAQ mesoscale modeling system is used, coupled with the MEGAN model for the processing of biogenic volatile organic compound emissions. A set of temperature perturbations (spanning from 1 to 5 K) is applied on a base case simulation corresponding to July 2004. The results indicate that the Eastern Mediterranean basin acts as a reservoir of pollutants and their precursor emissions from large urban agglomerations. During summer, chemistry is a major sink at these urban areas near the surface, and a minor contributor at downwind areas. On average, the atmospheric processes are more effective within the first 1000 m above ground. Temperature increases lead to increases in biogenic emissions by $9 \pm 3\%$ K^{-1}. Ozone mixing ratios increase almost linearly with the increases in ambient temperatures by 1 ± 0.1 ppb O_3 K^{-1} for all studied urban and receptor stations except for Istanbul, where a 0.4 ± 0.1 ppb O_3 K^{-1} increase is calculated, which is about half of the domain-averaged increase of 0.9 ± 0.1 ppb O_3 K^{-1}. The computed changes in atmospheric processes are also linearly related with temperature changes.

1 Introduction

Several meteorological variables, including temperature, precipitation and atmospheric ventilation impact air quality (e.g., Jacob and Winner, 2009). Among these variables, temperature is shown to have the largest effect on ozone (O_3) mixing ratios (Sanchez-Ccoyllo et al., 2006; Dawson et al., 2007). O_3 is a product of complex non-linear interactions between nitrogen oxides (NO_x) and volatile organic compounds (VOC) in the presence of sunlight (Crutzen, 1994; Seinfeld and Pandis, 1998). Depending on VOC/NO_x ratios, O_3 can be produced or consumed (Sillman and Samson, 1995). Temperature increases enhance biogenic emissions of isoprene and other VOCs as well as photochemical activity since most thermal atmospheric reactions show positive temperature dependence. Thus, temperature increases in the presence of sufficient NO_x lead to increases in O_3 levels.

The Eastern Mediterranean basin acts as a receptor of anthropogenic emissions from Europe, wind-driven dust from Sahara desert (Kanakidou et al., 2007, 2011), biogenic hydrocarbons from the surrounding vegetation (Liakakou et al., 2007) and sea-salt particles (Athanasopoulou et al., 2008). In addition, there are two important megacities in the region: Istanbul (~12 million inhabitants) and Cairo (~16 million inhabitants), as well as the large urban agglomerations like Athens (~4 million inhabitants), contributing to the anthropogenic emissions. The result is complex photochemistry and transport patterns leading to elevated levels of O_3 and particulate matter (PM) in the area (Gerasopoulos et al., 2006a, b; Kanakidou et al., 2011). Ground-based observations and satellite measurements show elevated amounts of O_3 over the Eastern Mediterranean during the last decade

(Vrekoussis et al., 2007). Gerasopoulos et al. (2005) reported high background O_3, particularly in spring and summer, attributed to meteorological conditions. These observations showed that while primary pollutant levels decrease downwind, secondary pollutants like O_3 are produced photochemically during transport of precursors downwind from the large agglomeration centers and from the surrounding regions: Europe, Balkans and north of the Black Sea. Pollution transported toward the Mediterranean is affected by local meteorological parameters like land-sea breeze circulations and orographic flows (Lelieveld et al., 2002). In addition to the near-surface long range transport (LRT) of pollutants, the high O_3 concentrations in the planetary boundary layer (PBL) are, partly attributed to entrainment from the free-troposphere. These pollution patterns have been observationally documented by several experimental studies; however the number of mesoscale modeling studies focusing on this area remains limited.
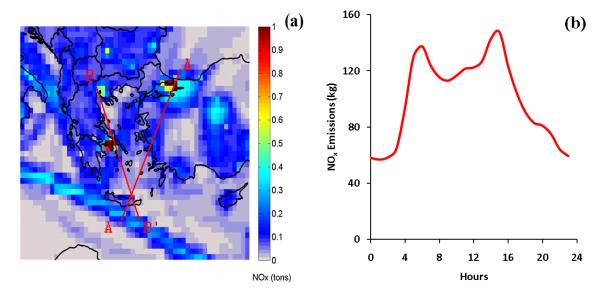
Chemistry and transport models (CTMs) can serve as fundamental tools to understand the complex and dynamic interactions between meteorology and chemistry at multiple temporal and spatial scales (Kindap et al., 2006; Kallos et al., 2007; Van Noije et al., 2004). Earlier modeling studies for the region pointed out the importance of local and regional circulations on air pollutant levels (Melas et al., 1998a, b). Poupkou et al. (2008) showed that the Athens urban plume significantly impacts the O_3 levels over the southern Aegean and Mediterranean. Lazaridis et al. (2005) applied the UAM-AERO model to simulate photo-oxidants and PM in the Eastern Mediterranean and indicated the importance of photo-oxidant and fine aerosols dynamics in the area as well as the significant contribution of regional transport to the observed pollution levels. Vegetation is a strong source of VOC emissions in the Mediterranean (Symeonidis et al., 2008). Poupkou et al. (2006) found that the biogenic emissions can lead to an increase of mean O_3 levels up to 10 ppb in Greece during summer while their impact on maximum ozone values is more pronounced leading to increases that can reach 20 ppb. Similar results for the Eastern Mediterranean are reported by Curci et al. (2009) modeling study for Europe. Recently, Im et al. (2011) evaluated a larger impact of biogenic emissions on the regional O_3 levels that can reach 25 ppb in the extended Istanbul area, where anthropogenic nitrogen oxide levels are high. These results demonstrate the importance of natural emissions on O_3 levels in the area. CTMs can also provide useful information on how changing meteorology may affect the pollutant concentrations (Tsigaridis et al., 2005; Dawson et al., 2007; Liao et al., 2009) as well as the physical and chemical processes leading to these concentration changes (Hogrefe et al., 2005; Goncavles et al., 2008), by employing scenarios that have perturbed meteorology and/or emissions.

The Mediterranean region is very sensitive to changes in climate (IPCC, 2007). Thus, future changes in climate and local meteorology can have significant impacts on the

natural emissions and regional air quality. In the present study, we investigate the potential impacts of increases in ambient temperature on air quality in the Eastern Mediterranean. We focus on the levels of O_3 and its precursors from 1–15 July 2004. For this purpose, the US EPA Community Multiscale Air Quality (CMAQ) chemistry and transport model driven by the Weather Research and Forecasting model (WRF-ARW) deduced meteorology is used and a number of temperature perturbation scenarios are performed. Models and scenarios are described in Sect. 2. The results are presented and discussed is Sect. 3. The contributions of various atmospheric processes within the surface layer and the PBL are analyzed. Focus is put on the effects of temperature changes on the biogenic emissions, photochemistry, and the atmospheric processes. Finally, the conclusions are given in Sect. 4.

2 Materials and methods

2.1 Meteorological model

In order to produce the meteorological fields necessary for the CMAQ model, WRF-ARW v3.1.1 has been used (Sharmock and Klemp, 2008). The WRF model is widely used by the mesoscale modeling community and has proven to give satisfactory results for the Mediterranean region (Borge et al., 2008; Im et al., 2010). The initial and boundary conditions have been provided from the National Centers for Environmental Prediction (NCEP) on $1° \times 1°$ horizontal and 6-h temporal resolution, with a vertical extent up to 10 mbar. The simulations have been carried out on a single domain that covers the Eastern Mediterranean region on a 30 km spatial resolution (Fig. 1). The domain has 58 and 47 grid cells on east-west and north-south directions, respectively, with 30 vertical layers. The lowest level is 8 m high and the domain top extends to ∼16 km. The model layer thickness increases from surface to the model upper boundary. PBL heights are calculated with the Meteorology-Chemistry Interface Processor (MCIP: Otte and Pleim, 2010) and PBL top is generally within the first 27 layers. The 27th layer corresponds to a height of about 3 km. The remaining 3 layers are very thick and their width extends from around 3 km from surface to 16 km. The physical options used in this study are WRF Single Moment 6-class microphysics scheme (Hong and Lim, 2006), RRTM (rapid radiative transfer model) longwave radiation scheme (Mlawer et al., 1997), Dudhia shortwave radiation scheme (Dudhia, 1989), NOAH land surface model (Chen and Dudhia, 2001), Yonsei University Planetary Boundary Layer scheme (Hong et al., 2004) and Kain-Fritsch cumulus parameterization scheme (Kain, 2004). Additionally, nudging has been applied for temperature, wind and moisture parameters towards the NCEP reanalysis for all model grids. The nudging coefficients are set to $0.0003\,\mathrm{s}^{-1}$ for each variable and forcing every 6 h has been applied.

Fig. 1. NO$_x$ emissions in the model domain: **(a)** spatial distribution of emissions integrated over the 15-day simulation period (tons grid^{-1}) and **(b)** diurnal profile of emissions (kg h^{-1}). The lines A–A$'$ and B–B$'$ show the cross-sections of Istanbul-Finokalia and Thessaloniki-Athens-Finokalia, respectively.

2.2 Emissions

The emission inventory used here is a compilation of regional and smaller scale emission inventories. The most important anthropogenic emission sectors in Greece as well as in the large urban agglomerations of Athens, Greece and Istanbul, Turkey have been quantified using real activity information as well as high resolution digital maps utilizing bottom-up methodologies.

The emission inventories for all anthropogenic sources have been originally compiled at 10 km resolution for Greece and at 2 km resolution for Athens (Markakis et al., 2010a, b). These inventories have been mainly based on the bottom-up approach using activity information and statistics for traffic loads on major roads, fuel consumptions of vehicles, off-road vehicles, various ship types, and stack measurements in industries. The remainder of the domain shown in Fig. 1a is covered by the emission inventory of French National Institute for Industrial Environment and Risks (INERIS) (https://wiki.met.no/cityzen/page2/emissions). This inventory is a re-gridded product of the emissions of the European Monitoring and Evaluation Programme (EMEP) database (http://www.ceip.at/). Emissions within each $0.5° \times 0.5°$ EMEP grid cell have been reallocated to a $0.1° \times 0.1°$ lon/lat grid using the high resolution (300 m) global land cover database of GlobCover (http://ionia1.esrin.esa.int/).

The Istanbul inventory (Im, 2009; Im et al., 2010) is the first high resolution emission inventory developed for this city (2 km resolution) and covers gridded and hourly resolved emission rates for carbon monoxide (CO), NO$_x$, sulfur oxides (SO$_x$), ammonium (NH$_3$), non-methane VOCs

(NMVOC) and particulate matter (PM$_{10}$ and PM$_{2.5}$). Emissions for a number of sources such as road transport, industrial and residential combustion and cargo shipping are calculated based on detailed information gathered from official sources of the municipality of Istanbul.

Finally the above mentioned individual emission inventories have been merged in order to meet the needs of this study for a 30 km resolution grid. All PM and NMVOC species are speciated into Carbon Bond 5 (CB5) species (Yardwood et al., 2005). The vertical distribution of emissions is calculated based on the Selected Nomenclature for Air Pollution (SNAP) codes provided by Simpson et al. (2003). A sample of the spatial distribution of the daily NO$_x$ emissions summed over all the sectors and averaged over the studied period are presented in Fig. 1a. This figure clearly depicts the elevated emissions over Istanbul and Athens. The shipping routes also stand out, pointing to a potentially significant environmental impact of ship emissions in the region. The mean diurnal variability of the emissions over the model domain is shown in Fig. 1b that demonstrates the clear peaks in the morning and evening rush hours, which are dominated by the road-traffic sector.

The biogenic emissions have been calculated using the Model of Emissions of Gases and Aerosols from Nature (MEGAN) module of the WRF-CHEM 3.1.1 online-coupled meteorology-chemistry model (Grell et al., 2005). Detailed description of the MEGAN model is provided in Guenther et al. (2006). This online version of MEGAN in WRF-CHEM model uses the same methodology with the offline version of MEGAN model 2.04 (Qian et al., 2010). MEGAN calculates 134 biogenic species, which are then mapped to 20 major

groups, including isoprene, monoterpenes, sesquiterpenes, oxygenated compounds, and other VOCs from terrestrial vegetation and nitrogen oxide (NO) from soils. CO emissions are also estimated by the model. The input files needed to run the MEGAN model include modified emission factors, satellite-derived vegetative cover, including Leaf Area Index (LAI) and Plant Functional Type (PFT) fractions, as well as climatological temperature and solar radiation for each grid cell. The WRF-CHEM model is modified to calculate all 20 MEGAN biogenic emission rates for each time step of the meteorology simulation. The emission rates are then converted to CB5 chemical species in order to be merged with the anthropogenic emissions for use in the CTM simulations. Mapping of individual NMVOCs to CB5 species has been based on the assignment matrixes and molecular weights described in Yardwood et al. (1999, 2005).

2.3 Chemistry and transport model

The CMAQ model version 4.7 has been used to simulate the atmospheric transport and the chemistry of the pollutants (Byun and Schere, 2006). CMAQ is a widely used model to simulate the atmospheric composition (Hogrefe et al., 2001; Unal et al., 2005; Kindap et al., 2006; Odman et al., 2007; Im et al., 2010). The boundary and initial conditions have been extracted from the Transport Model version 4 (TM4-ECPL) global chemistry- transport model. TM4-ECPL originates from the TM4 model (van Noije et al., 2004) to which emissions, chemistry and carbonaceous aerosol modules have been modified as described in detail by Myriokefalitakis et al. (2008, 2010, 2011) and references therein. TM4-ECPL model is able to simulate gas phase chemistry coupled with the major primary and secondary aerosol components including sulfate, nitrate and organic aerosols. The TM4-ECPL species have been mapped into CB5 species to be consistent with the other chemical input data, using the assignment factors described in Yardwood et al. (2005). The AERO5 module has been employed as the aerosol mechanism in CMAQ (Foley et al., 2010). This module also calculates sea-salt emission fluxes based on land-sea fractions in each grid cell, along with wind speed and relative humidity (Gong, 2003; Zhang et al., 2005). Yamartino scheme for advection (Yamartino, 1993) and asymmetric convective model (ACM2) scheme (Pleim, 2007) for vertical diffusion have been used in the study. The aqueous cloud chemistry has also been accounted for in the simulations (Foley et al., 2010). The horizontal and vertical resolution of the CMAQ model is identical to that of the WRF model, as described above.

The Integrated Process Analysis (IPR) tool of the CMAQ system has been employed to identify the dominant physical processes for 3 species/groups (O_3, NMVOCs and NO_x), at the surface (first model layer extending up to 8 m) and in the whole PBL, which extends up to $\sim$2.6 km that corresponds to the first 27 layers. Note that the PBL varies spatially and temporally (hourly) as presented in Fig. S1. IPR analysis

applications have been reported in the literature characterizing episodic events (San Jose et al., 2002; Gonçavles et al., 2009) as well as long-term (Zhang et al., 2006) and climatological simulations (Hogrefe et al., 2005). The atmospheric processes examined in IPR are horizontal and vertical transport, emissions of primary species, gas-phase chemistry, dry deposition, cloud processes and aerosol processes. Transport is calculated as the sum of advection and diffusion, horizontally (HTRA) and vertically (VTRA). Aerosol processes (AERO) include the effect of particle formation, condensation, coagulation and aerosol thermodynamics. Cloud processes (CLDS) are defined as the net effect of aqueous chemistry, below- and in-cloud mixing, cloud scavenging, and wet deposition. The weighted contributions of each process on O_3, NO_x and VOC levels have been estimated using Eq. (1), where PC_i is the individual contribution of the process i and $\% PC_i$ is the relative contribution of that process to the sum of the contributions from all the processes (Gonçalves et al., 2009).

$$\% \, PC_i = \frac{PC_i}{\sum_i abs(PC_i)} \times 100 \quad (1)$$

In the present study, we evaluate the major atmospheric processes (i): HTRA, VTRA, DDEP, and CHEM that determine O_3 mixing ratios.

2.4 Simulations

A number of scenarios have been simulated in order to evaluate the model system performance and the response in isoprene emissions, O_3 and its precursors concentrations to temperature changes in the Eastern Mediterranean. All simulations have been conducted for a 15-day period between 1–15 July 2004. The period was chosen based on the availability of isoprene measurements at the Finokalia air quality station in Crete. A spin-up period of 11 days has been used for all simulations, starting from 20 June 2004. However, the model results from this period have not been used in the model evaluations. The performed scenarios are as following:

1. The base case simulation (S0) has been conducted using the corresponding June and July 2004 meteorology.

2. Scenario S1 has been applied to estimate the possible impact of a homogeneous increase of air temperature by 1 K in the whole domain, both horizontally and vertically. This has been achieved in two steps: first, the MEGAN code was modified so that for each time step when the biogenic emissions are calculated, the surface temperature is increased by 1 K compared to the temperatures in S0. Second, the Meteorology-Chemistry Interface Processor (MCIP: Otte and Pleim, 2010) outputs, which are used as the meteorological inputs for the CMAQ model, are modified to have increased temperatures by 1 K throughout the modeling domain. Note

that only the effect of temperature changes on biogenic emissions is evaluated in this study. Potential changes in anthropogenic emissions with temperature due to evaporative VOC emissions have been neglected.

3. Scenario S2: same as S1 but for a 2 K increase.

4. Scenario S3: same as S1 but for a 3 K increase.

5. Scenario S4: same as S1 but for a 4 K increase.

6. Scenario S5: same as S1 but for a 5 K increase.

7. Scenario S6 has been used to investigate the impact of a realistic temperature field from a warmer year on the chemical composition in the area. For this purpose, the temperature field of the S0 scenario has been replaced by the temperature field of the year 2007. The replacement has been conducted at the NCEP input data to the WRF model. This enabled the simulation of the impact of this temperature change to the meteorological fields driving atmospheric transport and chemistry in the CMAQ model and to the biogenic emissions. Indeed, although there are no computed changes in soil properties (temperature and moisture), deposition velocities and wind speeds in scenarios S0 to S5, these parameters change in scenario S6 (Table S1 in the Supplement). The MEGAN module takes into account the air temperature and the incoming radiation. In scenarios S0 to S5, only the 2 m temperature input to the MEGAN module has been modified. However in S6, the whole meteorology is computed after perturbing the air temperatures, thus also impacting the radiation. Therefore, both parameters affect the biogenic emissions. In addition, CMAQ internally recalculates the precipitating and non-precipitating cloud fractions using the ambient air temperature, which leads to changes in cloud cover and relative humidity in each scenario (Table S1) that affect the photodissociation rates and wet removal of the atmospheric trace constituents. Figure S2 in the Supplement shows the difference of the new temperature fields of each scenario from the base scenario, averaged over the domain at each model layer.

2.5 Model performance metrics

The model performance has been analyzed by comparing the model results for the lowest model layer with surface observations at various locations in the model domain. A number of statistical parameters have been calculated to serve as metrics for how well the model reproduces the observations on a daily basis. The statistical parameters applied are correlation coefficient (r), mean normalized bias (MNB) and index of agreement (IOA). More information is provided in the supplementary material.

Isoprene observations at Finokalia, Greece (monitoring station of the University of Crete; Mihalopoulos et al., 1997)

Table 1. Air quality stations used to evaluate the model results.

Stations	Latitude (° N)	Longitude (° E)	Altitude (m a.s.l.)
IST			
Sarachane	41.05	29.01	16
ATH1			
Ag. Paraskevi	37.99	23.82	290
Zografou	37.97	23.79	245
ATH2			
Liosia	38.08	23.70	165
Thrakomakedones	38.14	23.76	550
THES			
Panaroma	40.59	23.03	363
Neochorouda	40.74	22.88	229
FKL			
Finokalia	35.20	25.40	250

during summer 2004 (Liakakou et al., 2007) have been used to evaluate isoprene simulations in the model. In addition, O_3 simulations have been evaluated using observations at Finokalia (Liakakou et al., 2007), at Sarachane monitoring station from the Air Quality Network of Istanbul Metropolitan Municipality (http://www.havaizleme.gov.tr/Default.htm), in Athens from the National Air Pollution Monitoring Network of the Hellenic Ministry of Environment Energy and Climate Change, and in Thessaloniki from the Air Quality Monitoring Network of the Region of Central Macedonia. These stations have been attributed to the model grid boxes. Observations from stations located in the same model grid have been first averaged to better represent the conditions in that grid and then compared with the model results. Urban core stations have not been included because the resolution of the model is not able to resolve spatially highly variable surface emissions. Based on the classification, 5 station groups are generated (see Table 1 and Fig. S3).

3 Results and discussion

3.1 Model evaluation

The model-calculated isoprene and terpene (monoterpenes and sesquiterpenes) emissions, summed over the 15-day simulation period are presented in Fig. 2. The south western parts of Greece, Turkey, and the Black Sea are characterized by relatively high isoprene and terpene emissions. For the 15-day simulation period, the model-calculated domain-wide isoprene emissions of 177 tons, largely exceed those of monoterpenes (49 tons) and sesquiterpenes (4 tons).
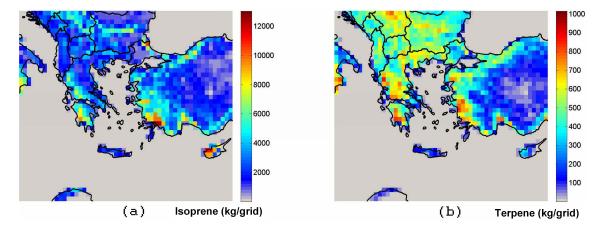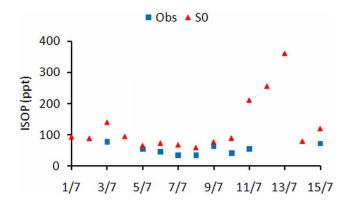
Fig. 2. (a) Isoprene and **(b)** terpene emissions (kg grid^{-1}) summed over the 15-day simulation period for the base case scenario (S0).

Table 2. Comparison of model-calculated (S0) surface hourly and daily mean isoprene and ozone mixing ratios with observations for the station groups.
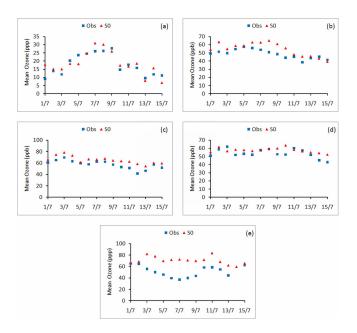
Parameters	Species	Hourly Variation					Daily Variation				
		IST	ATH1	ATH2	THES	FKL	IST	ATH1	ATH2	THES	FKL
Correlation	Isoprene	–	–	–	–	–	–	–	–	–	0.5
	Ozone	0.4	0.3	0.3	0.7	0.3	0.9	0.8	0.9	0.5	0.4
Mean Normalized	Isoprene	–	–	–	–	–	–	–	–	–	90.7
Bias (%)	Ozone	61	11	18	9	48	6.1	12.2	13.5	7.1	47.5
Index of	Isoprene	–	–	–	–	–	–	–	–	–	0.3
Agreement	Ozone	0.6	0.5	0.6	0.8	0.4	0.9	0.7	0.7	0.6	0.4

α- and β-pinenes are calculated to be the major monoterpene species (57%). β-caryophyllene contribute by 60% to the total sesquiterpene emissions. Note, however, that uncertainties of a factor of 3–5 are associated with the biogenic emission estimates (Simpson et al., 1999; Smiatek and Steinbrecher, 2006; NATAIR, 2007). These uncertainties may originate from a number of sources including the plant-specific emission potentials, the vegetation type and the associated biomass, the impact of various climate parameters like temperature, radiation, humidity and greenhouse gases, and chemical processes that determine the emissions of VOC in the canopy (Guenther et al., 2006; Arneth et al., 2007; Poupkou et al., 2010). For July 2003, Steinbrecher et al. (2009) used different modeling approaches in order to estimate the biogenic emissions over Europe and calculated differences of a factor of 1.3 for the isoprene emissions and a factor of 3.3 for the terpene emissions. For the same period, Poupkou et al. (2010) found a good agreement in total isoprene emissions (a factor of 1.2) between the Biogenic Emission Model (BEM) and the MEGAN model (Guenther et al., 2006).

Due to the above-mentioned high uncertainties in biogenic emissions, simulated isoprene concentrations may also differ significantly from observations, particularly in remote regions such as Finokalia (FKL), which represents a back-

ground station in the Eastern Mediterranean. Earlier studies for the Eastern Mediterranean including comparison between observed and simulated isoprene concentrations are very limited. Poupkou et al. (2010) applied the BEM model coupled with the CAMx chemistry and transport model (ENVIRON, 2006) for Europe in 30 km spatial resolution for the summer in 2003. They evaluated BEM/CAMx calculated isoprene concentrations with the available EMEP network data and found agreement within a factor of 2–4, depending on location. In our study, the WRF-MEGAN/CMAQ model (S0) overestimates the isoprene mixing ratios at FKL by a factor of 2 (91%), which results in a low IOA value of 0.3 (Table 2). The isoprene temporal variation is captured moderately with a correlation coefficient of 0.5 (Fig. 3, Table 2). In the present study, the temporal variation of daily mean O_3 mixing ratios calculated by the CMAQ model agree moderately with observations at FKL ($r = 0.4$) and THES ($r = 0.5$) and much better at IST ($r = 0.9$) and ATH ($r = 0.8 - 0.9$) (Table 2). Figure 4 shows the comparison of calculated daily mean O_3 mixing ratios with available observations at all station groups. Particularly at IST and ATH2, temporal variability is successfully reproduced ($r = 0.9$). On the other hand, the mixing ratios are overestimated at all stations, ranging from 7.4% (THES) to 47.9% (FKL). As seen in Table 2,

Fig. 3. Observed (squares) and modelled (triangle) daily mean isoprene mixing ratios at Finokalia station (FKL).

Fig. 4. Observed (square) and modelled (triangle) surface daily mean O$_3$ mixing ratios at **(a)** IST, **(b)** ATH1, **(c)** ATH2 **(d)** THES and **(e)** FKL station groups (For station details, see Table 1).

hourly variations are not captured as well as the daily variations. These differences can be attributed to many sources of uncertainties, particularly the emissions and their spatial resolution that imply a potentially underestimated O$_3$ titration by reactions with NO$_x$. In addition, isoprene mixing ratios are overestimated by a factor of 2 at FKL, which also has an impact on the O$_3$ production. The overestimation of O$_3$ at FKL can be partially due to underestimated O$_3$ removal through dry deposition within the corresponding grid cell that is covered largely by water. The better performance of the model (IOA = 0.9) for the Istanbul region is attributed to the updated high resolution anthropogenic emissions inventory developed recently for Istanbul and adopted here (Im, 2009).

The mean surface distributions of O$_3$, NO$_x$, CO and OH mixing ratios and the molar VOC/NO$_x$ ratios (calculated as the ratio of NMVOCs to NO$_x$) are presented in Fig. 5. Lower O$_3$ mixing ratios are calculated for IST ($\sim$19 ppb) than for Athens ($\sim$50 ppb) due to the O$_3$-titration by high NO$_x$ emissions taking place in this megacity, as clearly seen in Fig. 1. The impact of the Athens urban plume on the southern Aegean Sea air quality (Fig. 5a) is demonstrated in agreement with the findings of Poupkou et al. (2009). It is also clear that shipping emissions are an important anthropogenic source of NO$_x$ in this region (Fig. 5b), in agreement with earlier studies (Athanasopoulou et al., 2008). Poupkou et al. (2008) calculated the maritime transport emissions contribution to O$_3$ levels at approximately 20 ppb on the coastlines of southern and western Greece, while in the regions influenced by high amounts of nitrogen oxides emitted from the sea transport activities, the O$_3$ concentrations were suppressed. On the other hand, due to the higher NMVOC and lower NO$_x$ emissions in Athens (annually 93 and 78 ktons, respectively: Markakis et al., 2010a), than in Istanbul (annually 77 and 305 ktons, respectively: Im, 2009), higher VOC/NO$_x$ ratio and O$_3$ mixing ratios are calculated in Athens (Fig. 5e). The OH distribution indicates a higher oxidative capacity of the Athens atmosphere than over Istanbul. This can be attributed to higher NMVOC emissions and in general, faster thermal reactions in the troposphere, since most of them show positive temperature dependence. Due to warmer temperatures, this results in more and faster reacting organic compounds in the atmosphere and leads to more intensive chemical activity over Athens.

The model-calculated molar CO/NO$_x$ ratios are compared with the observations from measurement networks at IST, ATH and THES. The CO/NO$_x$ ratio is an indicator of emission composition and air mass ageing. Due to the short lifetime of NO$_x$ compared to CO, low CO/NO$_x$ ratios indicate high contribution by local emissions whereas high ratios point to important contribution of transported air masses. The distribution of CO/NO$_x$ molar ratios at surface, computed for simulation S0 and averaged over the simulation period, is depicted in Fig. 5f. The model-calculated CO/NO$_x$ ratios increase from below 50 in the large agglomerations to above 150 downwind, due to influence from the surrounding region, which is consistent with the observed pattern (Kanakidou et al., 2011). The low ratio in Istanbul indicates significant local influence whereas in Athens, regional influence is much stronger. Finally, Finokalia is subject to the largest regional influence. The model highly underestimates the CO/NO$_x$ ratio in Istanbul by a factor of 4 (2.9 vs. 15.5), whereas in Athens agreement is much better (14.2 vs. 14.6). In Istanbul, the large difference can be attributed to the uncertainty in the road-transport emissions. At THES, the model-calculated CO/NO$_x$ molar ratio is in good agreement with the observations with a slight overestimation (24.9 vs. 21.2). Due to the lack of observations at FKL for the studied period, the model-calculated ratio is compared with the annual
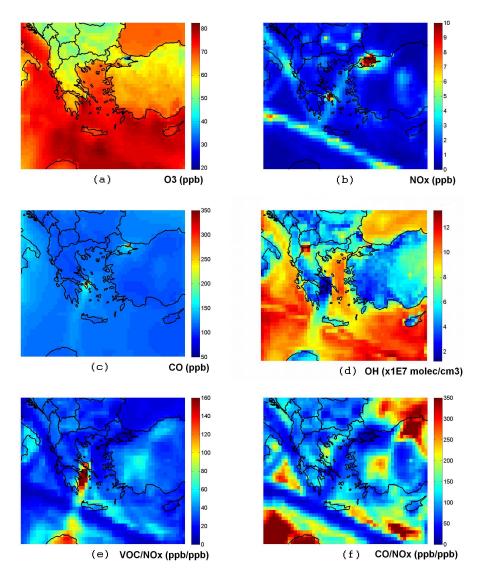
Fig. 5. Modelled distributions of mean surface **(a)** O$_3$, **(b)** NO$_x$, **(c)** CO, **(d)** OH mixing ratios, and **(e)** molar VOC/NO$_x$ and **(f)** molar CO/NO$_x$ ratios in the base case scenario (S0) averaged over the 15-day simulation period.

average ratio provided by Kanakidou et al. (2011). At FKL the model calculates a CO/NO$_x$ ratio of 125 whereas measurements provide values between 100 and 300.

3.2 Process analyses

The IPR analysis calculates the mass concentration fluxes from each atmospheric process that affects the concentration of the individual species. These flux values are then divided by the sum of the absolute values for each process to get the % contribution of the respective process. The present IPR analysis focuses on the relative contributions of HTRA, VTRA, DDEP and CHEM processes to O$_3$ concentrations at different vertical levels in PBL. For the whole modeling domain (not shown here), the S0 simulation results show that VTRA is the major source term of surface O$_3$ (50%) and

DDEP is the major sink (48%). HTRA and CHEM have relatively very low contributions to O$_3$ levels. On the other hand, in the entire PBL, the calculations show that chemistry is a more important source term (7%) than at surface. VTRA is still the major source term (43%) and DDEP the major sink term (29%). HTRA is an important sink of O$_3$ (21%) since O$_3$ is exported horizontally out of the domain.

The IPR analyses are employed for individual station groups within the surface layer and PBL, as well as each vertical layer within the PBL, in order to better understand the different physical and chemical processes affecting the atmospheric composition in these cities. Note however that the surface layer is rather thin (8 m) and, therefore, it is expected to be strongly affected by deposition (DDEP and convection (VTRA) processes, more than the overlaying layers. Thus, the process analysis is performed both for the surface layer

Table 3. Relative per cent contributions of individual atmospheric processes to O$_3$, NO$_x$ and NMVOC levels in the base case scenario (S0) for individual station group (See Table 1 for station details). HTRA stands for horizontal transport, VTRA for vertical transport, DDEP for dry deposition, CHEM for gas-phase chemistry and CLDS for cloud processes and aqueous-phase chemistry.
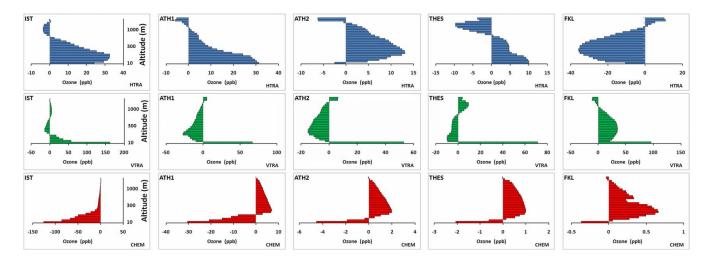
| | Station Groups | | | | | | | | | |
| | IST | | ATH1 | | ATH2 | | THES | | FKL | |
	Surface	PBL	Surface	PBL	Surface	PBL	Surface	PBL	Surface	PBL
Ozone										
HTRA	6.5	27.9	15.9	49.6	−2.3	44.7	6.1	22.2	−5.4	−42.7
VTRA	43.5	22.1	34.1	−37.2	50.0	−37.7	43.9	19.2	49.9	49.4
DDEP	−16.2	−5.3	−34.5	−12.8	−43.4	−12.2	−48.7	−50.0	−44.4	−7.3
CHEM	−33.8	−44.7	−15.5	0.4	−4.3	5.4	−1.3	8.7	−0.2	0.6
NO$_x$										
HTRA	−1.1	−10.5	−0.6	−6.3	0.3	3.4	0.2	0.4	−1.4	−23.3
VTRA	−47.8	−37.4	−47.4	−36.0	−47.9	−39.1	−47.9	−42.3	−46.4	−16.8
DDEP	−0.9	−0.9	−0.6	−0.6	−0.7	−0.7	−1.8	−1.7	−1.5	−1.1
CHEM	−0	−0.6	−1.4	−7.1	−1.4	−10.2	−0.3	−6.0	−0.7	−8.4
EMIS	50.0	50.0	50.0	50.0	46.7	46.6	49.8	49.6	50.0	50.0
CLDS	−0.1	−0.5	−0	−0	−0	−0.1	−0	−0	0	−0.5
VOC										
HTRA	−1.6	−13.4	−0.7	−8.7	0.9	5.1	0.6	2.2	0.9	5.1
VTRA	−45.8	−33.3	−47.9	−39.7	−48.1	−47.3	−46.6	−43.3	−48.1	−47.3
DDEP	−2.5	−2.4	−1.4	−1.4	−1.9	−1.7	−2.8	−2.6	−1.9	−1.7
CHEM	−0	−0.4	−0	−0.2	−0.1	−0.9	−0.6	−4.1	−0	−0.9
EMIS	50.0	50.0	50.0	50.0	49.1	45.0	49.4	47.7	49.2	45.0
CLDS	−0.1	−0.5	−0	−0	−0	−0.1	−0	−0	−0	−0

alone and for the entire PBL. The IPR results for each station group presented in Table 3 show that at the surface layer VTRA is the major source term for all station groups, contributing more than 40% except at ATH1 (34%) and at ATH2 (50%). DDEP and CHEM are sink terms of O$_3$ at all station groups. Where chemical destruction of O$_3$ is dominant, DDEP becomes less pronounced (IST and ATH1). These station groups are located in the emission hot spots and O$_3$ is titrated rapidly by fresh NO emissions. In the entire PBL, VTRA is still a major source of O$_3$ at FKL, IST and THES. However, at both ATH1 and ATH2, VTRA becomes a sink with height, suggesting an updraft of the air parcels carrying the pollutants to higher altitudes. At these two station groups, HTRA becomes very effective in the PBL carrying O$_3$ to the station groups. CHEM is more pronounced in the PBL than at the surface layer, particularly at the IST, where removal through chemical destruction (titration by NO$_x$) is even higher (−44.7%) than at the surface layer (−33.8%), and at ATH1. At both ATH1 and ATH2, CHEM is a sink at the surface layer and becomes a weak source of O$_3$ when the entire PBL is considered.

HTRA can be as significant as VTRA within the entire PBL. Since dry deposition occurs at the surface layer only, its contribution is smaller when analyzing the whole PBL.

As presented in Fig. 6, the contributions of all HTRA, VTRA and CHEM are more pronounced in the first ∼1000 m above the surface. At FKL, HTRA is a sink term up to around 1000 m, and a source term above 1000 m. O$_3$ is transported downwards FKL within the first 1000 m and upward above. At IST, VTRA is a source for O$_3$ in the first 100 m, whereas between 100 and 500 m, it is a sink for O$_3$ since O$_3$ is carried away from IST and towards higher altitudes. The IST area is a region where O$_3$ is chemically destroyed by fresh NO$_x$ emissions throughout the entire PBL. The effect is particularly significant in the first 100–200 m above ground, where in addition to the domestic combustion, traffic and shipping emissions are extremely effective. O$_3$ is horizontally transported to both ATH1 and ATH2. While HTRA is effective in the first 1000 m of PBL over ATH1, O$_3$ is advected away from ATH2 in the first 20 m whereas there is an O$_3$ influx to the station group at higher altitudes.

As presented in Table 3, local emissions (EMIS) are the main sources of NO$_x$ and NMVOCs at all station groups, whereas VTRA is the dominant sink, different from the case for O$_3$. VTRA leads to the mixing of the air masses from the surface with above through turbulence and convection. VTRA transports high O$_3$ from above downwards, and surface emissions and precursors (NO$_x$ and NMVOCs)

Fig. 6. Process contributions to O$_3$ concentrations in station groups for each vertical layer of the PBL: First row presents horizontal transport (HTRA), second row vertical transport (VTRA) and third row chemistry (CHEM). Units are ppb/15 days of simulation.
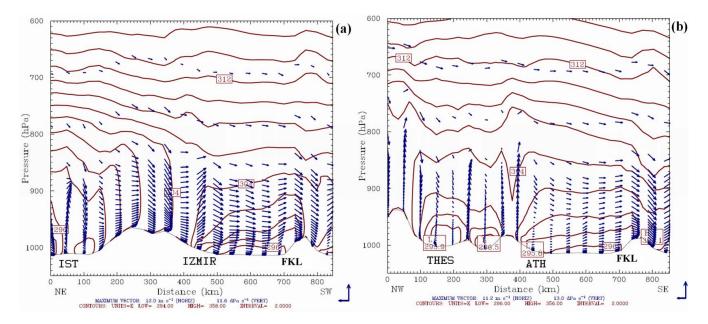

Fig. 7. Circulation vectors along **(a)** Istanbul-Finokalia (A-A') axis and **(b)** Thessaloniki-Athens-Finokalia (B-B') axis at 12:00 UTC, 2 July 2004.

upwards. HTRA is more effective in the entire PBL compared to the surface layer for both NO$_x$ and NMVOC. DDEP is not an important sink term for these species as it is for O$_3$. Generally, all station groups are subject to more effective contribution of HTRA in the entire PBL than at the surface layer that results in a relative decrease of VTRA impact on all species.

A snapshot of the horizontal and vertical circulation patterns in the area is given in Fig. 7 showing the circulation vectors, along with potential temperatures in the two cross-sections. The first cross-section cuts across the Istanbul-Finokalia axis (A-A') while the second cross-section cuts across Thessaloniki-Athens-Finokalia axis (B-B') (Fig. 1). In both cross-sections, northerly flow is prevailing in the modeling domain. The horizontal winds are stronger in the A-A' cross-section which is closer to the axis of the Etesian winds (Fig. 7a) compared to the winds in the B-B' cross-section (Fig. 7b). In Istanbul (Fig. 7a), the air parcels move upward until around 850 mbar. This pattern is consistent with the existence of the two convective cells driven by the heat island effect of the megacity, as described in Ezber et al. (2007). The upward motion carries the air pollutants
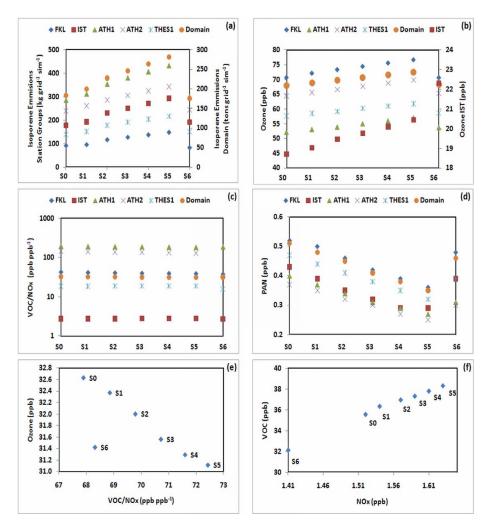
Fig. 8. Simulated **(a)** total isoprene emissions, **(b)** mean ozone, **(c)** mean molar VOC/NO$_x$ ratio, **(d)** mean PAN, **(e)** mean molar O$_3$ vs. VOC/NO$_x$, and **(f)** mean VOC vs. NO$_x$ for each station group and the domain; for the simulation period of 15 days.

emitted over Istanbul to higher altitudes, facilitating their long distance transport. Although the updraft is stronger over Athens, where it is enhanced by the topography (Fig. 7b), part of the air parcels carrying the city's pollutant emissions are captured in the sea breeze circulation and are transported back to the city (vertical recirculation, Melas et al., 2005). However, some of the air parcels are lifted to higher altitudes from where they can be transported southwards. Polluted air masses finally subside over Crete. It should be noted that a 30 km spatial resolution may not be enough to accurately resolve the local circulations in the area. Our results are consistent with previous studies: Gerasopoulos et al. (2005, 2006b) analysing 7-year observations of O$_3$ from Finokalia have identified transport from Europe as the main mechanism that controlled O$_3$ levels, particularly in summer. Similarly, Vrekoussis et al. (2007) showed that northerly transport was a major contributor to nitrate (NO$_3$) levels, along with O$_3$, during summer. They have proved that intrusion

Table 4. Domain mean changes with respect to base case simulation in response to scenarios. Emission changes are integrated over the 15-day simulation period. Concentration changes are the mean changes over the same period.

Species (Units)	Change in Scenarios					
	S1	S2	S3	S4	S5	S6
Isoprene Emissions (tons)	16.3	44.5	62.7	80.6	98.0	−7.5
Monoterpene Emissions (tons)	5.1	12.3	18.7	25.7	33.5	−0.7
Sesquiterpene Emissions (tons)	0.8	2.1	3.3	4.7	6.4	−0.2
Ozone (ppb)	1.0	1.9	2.8	3.7	4.5	0.4
NO$_x$ (ppb)	0.1	0.1	0.1	0.1	0.1	−0.1
VOC (ppb)	0.8	1.5	1.8	2.3	2.8	−3.4

from the free troposphere and mass transfer in lower altitudes from polluted Europe, were significant sources in the Eastern Mediterranean.

3.3 Scenario analyses

The effect of temperature changes on isoprene emissions is depicted in Fig. 8a. This figure shows a quasi-linear positive response of isoprene emissions to increase in temperature. Domain-wide, increases of ambient temperatures by 1 to 5 K lead to $9 \pm 3\%$ K^{-1} increases in isoprene emissions. A similar pattern is also seen at the individual station groups, varying from $7.4 \pm 1.7\%$ K^{-1} at ATH2 to $10.6 \pm 4.7\%$ K^{-1} at IST. Table 4 provides the changes in domain-wide biogenic emissions (isoprene, monoterpenes and sesquiterpenes) and ozone, NO_x and VOC mixing ratios relative to the base case scenario, for the 15-days simulation period. Terpene emissions demonstrate a similar pattern to isoprene emissions, having the largest response to the 2 K increase in temperature.

Scenario S6 provides a domain wide decrease of isoprene emissions by 4.1% (Table 4) due to the lower temperatures applied over land compared to S0. However, for the whole domain, an average increase of 0.07 K exists at the surface. At Finokalia, 10% lower isoprene emissions are calculated compared to S0, whereas higher isoprene emissions are calculated at the other station groups (1.8% to 7.7%). Terpene emissions also decrease in scenario S6.
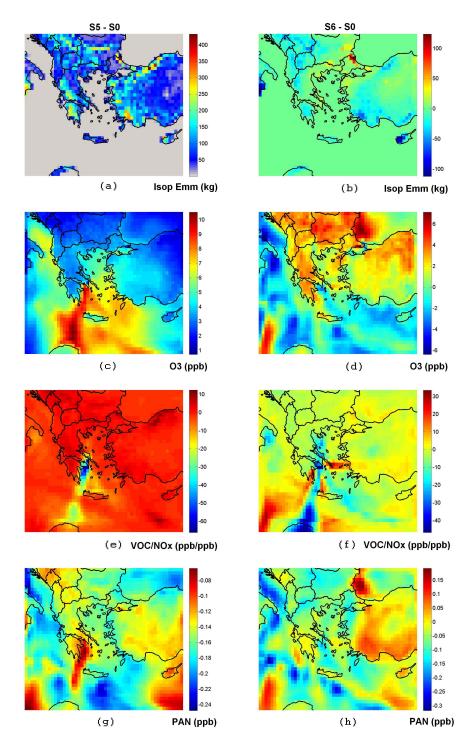
The increase in isoprene emissions together with photochemistry enhanced by the higher temperatures and the higher photolysis rates due to decreased cloud cover (90% K^{-1}) result in higher O_3 mixing ratios corresponding to a domain-mean increase by 0.9 ± 0.1 ppb O_3 K^{-1} (Fig. 8b). CMAQ calculates a correction factor to the clear-sky photo dissociation rates based on the cloud cover that, as presented in Table S1, changes in each scenario. Therefore, increase in temperature leads both to faster thermal reactions and higher photo dissociation rates, resulting in more intense chemistry. All station groups experience a quasi linear positive response to temperature changes for O_3 mixing ratios; that is 0.4 ± 0.1 ppb O_3 K^{-1} at IST, 1 ± 0.1 ppb O_3 K^{-1} at ATH1, 1.1 ± 0.1 ppb O_3 K^{-1} at ATH2, 0.9 ± 0.1 ppb O_3 K^{-1} at THES and 1.2 ± 0.2 ppb O_3 K^{-1} at FKL. The domain mean VOC/NO_x molar ratio decreases by $0.9 \pm 0.3\%$ K^{-1} (Fig. 8c), although both NO_x and VOC mixing ratios are enhanced with increasing temperatures. This is because the rate of increase in NO_x mixing ratios is calculated to be much faster than that of VOCs. The NO from soil activity is also increasing as calculated by the MEGAN model and contributes to the NO_x mixing ratios. Regarding the station groups, FKL, ATH1 and ATH2 experience VOC/NO_x ratio decreases by 1.9 ± 0.8, 1.4 ± 0.5 and $2.4 \pm 0.7\%$ K^{-1}, respectively; whereas IST and THES experience increases in VOC/NO_x ratios by 0.4 ± 0.3 and $0.4 \pm 0.2\%$ K^{-1}, respectively. PAN mixing ratios decrease by 0.03 ± 0.01 ppb K^{-1} on average in all simulations and at all station groups, as well as in the whole domain (Fig. 8d). This change is due to the enhanced decomposition of PAN to NO_2, which can then form O_3 (Sillman and Salmon, 1995; Dawson et al., 2007).

In the scenario S6, an increase of domain mean O_3 by 0.42 ppb is calculated. The highest change is calculated at IST (+3.6 ppb) whereas for ATH1, the mean O_3 is enhanced by 1.54 ppb, at ATH2 0.84 ppb and THES 0.97 ppb. At FKL, O_3 levels decrease by 0.05 ppb. The domain-mean molar VOC/NO_x ratio decreases by 3.7%. The smallest effects occur in the hotspot areas of IST and ATH1 (0.4 and 4.4%, respectively), whereas other station groups experience larger decreases (−11.8% in FKL, −13.4% at ATH2 and −15.4% at THES). PAN also decreases by 0.05 ppb domain wide, whereas FKL and IST experience a PAN decrease of 0.04 ppb, ATH1 0.09, ATH2 0.07 and THES 0.08 ppb. The changes in S6 are also due to the changes in meteorological variables, such as wind, soil properties and deposition velocities that lead to different transport and deposition patterns (Table S1).

The spatial distributions of changes in isoprene emissions and resulting O_3, VOC/NO_x ratios and PAN mixing ratios at the surface in scenarios S5 and S6 are presented in Fig. 9. This figure clearly shows the large changes in the Athens urban plume in scenario S5 compared to the base case (S0) due to a homogeneous warming in the atmosphere. On the other hand, due to the different modified meteorological fields in the S6 scenario, the changes are more scattered around the domain. The largest changes around Athens are due to the enhancement of NMVOC emissions by increasing temperatures, thus producing more O_3 downwind.

The impact of a 5 K temperature increase (S5) on the vertical distribution of O_3 at FKL, IST and ATH1 stations is presented in Fig. 10. The figure shows that in the emission hot spots IST and ATH1, there is a significant change in O_3 mixing ratios with height compared with the downwind site FKL, where the change is less pronounced. This can be attributed particularly to the intensity of the traffic emissions in the urban sites where they destroy ozone. The impact over IST is larger than over ATH1 due to the very large NO_x emissions. The O_3 mixing ratios are very similar (~72 ppb) around 4000 m at all stations, indicating a high free-tropospheric O_3 background over the entire region. The difference in simulated O_3 mixing ratios between scenarios S5 and S0, averaged over the PBL is calculated to be 5.1 ppb for FKL, 3.6 ppb for IST and 5.3 ppb for ATH1. However, these changes are not uniform throughout the vertical extent of the model (Fig. 10).
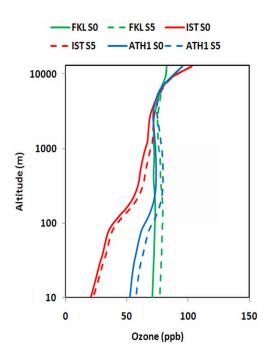
The budget term responses of surface and PBL O_3 in the model domain and at IST, ATH1 and FKL for each scenario are depicted in Fig. 11. At the surface layer and for the model domain (Fig. 11a), the changes in the mass fluxes associated with various processes for the different scenarios are almost linear with the temperature increases, except for S6. The largest change in VTRA is calculated for S6 (1.68 ppb for 15 days of simulation), which leads to a change very similar to S5 (1.66 ppb for 15 days of simulation), where the temperature is increased by 5 K. The HTRA is a source term at all stations considering the surface layer, except for ATH2

Fig. 9. Spatial differences between simulations S5 and S0 (S5–S0; left panel) and between simulations S6 and S0 (S6–S0; right panel) averaged over the 15-day simulation period in: **(a, b)** isoprene emissions; **(c, d)** surface ozone; **(e, f)** surface molar VOC/NO$_x$ ratios and **(g, h)** surface PAN.

and FKL. The temperature increases enhance the amount of O$_3$ transported to or from the station groups due to increased production of O$_3$. On the other hand, considering the entire PBL, ATH2 also becomes a receptor of O$_3$

transport. The contribution of HTRA is enhanced with increasing temperatures in the PBL, as it is the case for the surface layer. O$_3$ removal at the surface layer through HTRA increases linearly by 0.02 ± 0.01 ppb K^{-1} over the simulation

Fig. 10. Change of O_3 with altitude in base simulation (S0: solid lines) and plus 5 simulation (S5: dashed lines) for FKL, IST and ATH1 station groups for the simulation period of 15 days.

period, whereas this increase is 0.45 ± 0.06 ppb K^{-1} in the PBL (Fig. 11b). The contribution of VTRA on O_3 is enhanced by 0.33 ± 0.03 ppb K^{-1} at the surface layer and 0.10 ± 0.06 ppb K^{-1} in the PBL. The results point that temperature increases also enhance the dry deposition of O_3 by 0.37 ± 0.03 ppb K^{-1} due to increases in ozone mixing ratios. The largest change in DDEP is calculated for S5 (1.84 ppb). Less O_3 is removed by CHEM when temperatures increase (-0.05 ± 0.01 ppb K^{-1} at the surface layer and -0.72 ± 0.10 ppb K^{-1} in the entire PBL). This suggests that although chemical production of O_3 is enhanced in higher temperatures, destruction still dominates over production leading to a net destruction of O_3. Scenario S6 is an exception, where more O_3 is removed compared to the base case (0.04 ppb at the surface layer and 1.7 ppb in the PBL). The results indicate that the largest changes in VTRA for the 15 days of simulation occur in S6 (5.4 ppb). The responses are again linear with the temperature increases, except for S6.

Results of the IPR analyses conducted for FKL, IST and ATH1 on vertical basis are also presented in Fig. 11. Overall, the figure shows that scenario S6 behaves differently with respect to budget terms of O_3 than the other scenarios. At the surface layer, the largest difference in HTRA occurs at ATH2 for scenario S6. Considering the entire PBL, the largest change is calculated at ATH1 in scenario S6. All scenarios for the other station groups show similar results for VTRA at the surface layer. Considering the surface layer,
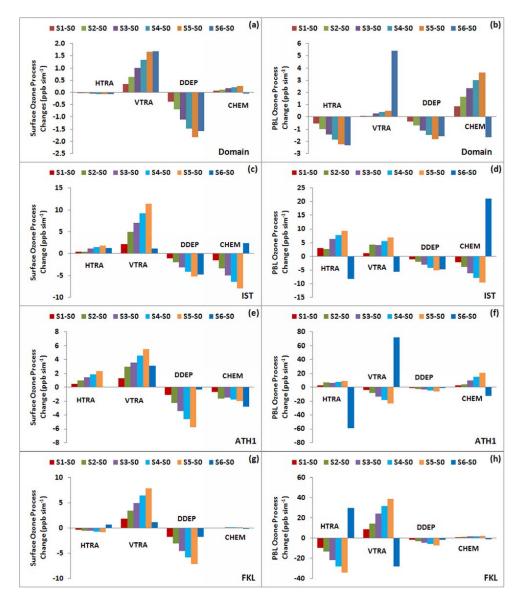
the largest differences occur at IST group, whereas within the entire PBL, FKL experiences the largest changes for VTRA. DDEP is a major sink term for all stations and scenarios, expect for S6, where the removal through dry deposition decreases compared to base case scenario. Chemistry is a major sink term in emission hot spots of IST and ATH1. At the surface layer, for both station groups, a loss of O_3 through chemistry is calculated, IST being the largest affected group. On the other hand, scenario S6 leads to decreased removal of O_3 in IST. A similar pattern is seen for the PBL, where loss through chemistry increases with increasing temperatures. The O_3 production through chemistry increases in PBL for all other station groups. The circulation pattern analysis together with the IPR analyses supports the previous observation-based findings that suggest the importance of transport for the air pollutant levels in the region.

4 Conclusions

The summer time O_3 concentrations and the processes governing these levels in the Eastern Mediterranean have been studied using the WRF/CMAQ modeling system coupled with the MEGAN model for the biogenic emission calculations for the summer in 2004. The impact of ambient temperature on O_3 concentrations and the involved processes has been investigated through temperature perturbations. The model system is able to simulate the observed isoprene concentrations at Finokalia station with an overestimation by a factor of two, which is within the uncertainty margin reported in previous studies for Europe, and better than the factor of 4 that represents an average limit of uncertainty in calculations of isoprene emissions in Europe.

O_3 concentrations are also satisfactorily simulated particularly at Istanbul and Athens station groups, whereas the model performed moderately for Finokalia and Thessaloniki station groups. The horizontal resolution of the model (30 km × 30 km) imposes limitations in its ability to simulate the sharp gradients in the emissions between the urban centers and the surrounding rural locations. As a consequence, urban center modelled emissions might be underestimated whereas those in the surrounding location might be overestimated. This is expected to result in an underestimation of O_3 titration by NO_x in the urban centers and an overestimation in the close-by surrounding regions. There is an O_3 overestimation of 48% at Finokalia station, which might be related to underestimation of dry deposition in the particular model grid cell that is largely covered by water. At other locations, the model overestimates the observations by 10% on average, which is acceptable given the coarse resolution of the model.

On a regional basis, the IPR results show that transport is largely responsible for the O_3 levels in the Eastern Mediterranean basin. Chemistry plays a minor role in downwind areas but is a major sink at urban cores near the surface. On the other hand, chemistry is a source term within the PBL with a

Fig. 11. Differences of mass fluxes between the perturbation simulations and the base case simulation for the surface layer (left panel) and for the entire PBL (right panel) in **(a, b)** model domain; **(c, d)** IST; **(e, f)** ATH1 and **(g, h)** FKL (units are ppb over the simulation period of 15 days).

more pronounced effect compared to the surface layer. The IPR results show that O_3 and its precursors are carried from high altitudes and subside over the Mediterranean basin. The precursor emissions are transported away from the sources through both horizontal and vertical transport whereas they chemically destroy O_3 by reacting with NO in the urban areas. VOCs are transported away from these sources and lead to production of O_3 at further downwind areas. O_3 then sinks over the Mediterranean basin due to subsidence. The circulation patterns produced by the WRF model also agree with the findings of the CMAQ/IPR analyses, clearly showing the northerly transport and the subsidence over Crete. They also point to the involvement of local circulations in amplifying

the impact of local emissions over the coastal urban agglomerations.

Isoprene emissions and O_3 concentrations respond almost linearly to temperature increases. The increase in ambient temperatures leads to a domain wide increase of isoprene emissions by $9 \pm 3\%\,\mathrm{K^{-1}}$. An ozone increase of $0.9 \pm 0.1\,\mathrm{ppb}\ O_3\,\mathrm{K^{-1}}$ is calculated for the whole model domain. Simulated PAN concentrations are decreasing with increasing temperatures, which in return results in increasing NO_2 levels that produce more O_3.

Although forecasted meteorological fields would provide more realistic responses of air pollutants to changes in climate, the results of the present study clearly show that the

ozone levels in the Eastern Mediterranean are subject to increase with the increasing isoprene emissions in a warmer future climate. Relatively small changes (0.9 ± 0.1 ppb O_3 K^{-1} as computed here) might contribute to summer time exceedences at the downwind areas in the Eastern Mediterranean. While developing air pollution mitigation options, possible future changes in the climate have to be taken into account.

Supplementary material related to this article is available online at: http://www.atmos-chem-phys.net/11/3847/2011/ acp-11-3847-2011-supplement.pdf.

Edited by: M. Gauss

References

Athanasopoulou, E., Tombrou, M., Pandis, S. N., and Russell, A. G.: The role of sea-salt emissions and heterogeneous chemistry in the air quality of polluted coastal areas, Atmos. Chem. Phys., 8, 5755–5769, doi:10.5194/acp-8-5755-2008, 2008.

Borge, R., Alexandrov, V., del Vas, J. J., Lumbreras, J., and Rodriguez, E.: A comprehensive sensitivity analysis of the WRF model for air quality applications over the Iberian Peninsula, Atmos. Environ., 42, 8560–8574, 2008.

Byun, D. and Schere, K. L.: Review of the governing equations, computational algorithms, and other components of the Models-3 Community Multiscale Air Quality (CMAQ) modeling system, Appl. Mech. Rev., 59, 51–77, 2006.

Chen, F. and Dudhia, J.: Coupling an advanced land-surface/hydrology model with the Penn State/ NCAR MM5 modeling system. Part I: model description and implementation, Mon. Weather Rev., 129, 569–585, 2001.

Crutzen, P. J.: An overview of atmospheric chemistry, European Research Course on Atmospheres (ERCA), Topics in: Atmospheric and Interstellar Physics and Chemistry, edited by: Boutron, C. F., 63–88, 1994.

Curci, G., Beekmann, M., Vautard, R., Smiatek, G., Steinbrecher, R., Theloke, J., and Friedrich, R.: Modeling study of the impact of isoprene and terpene biogenic emissions on European ozone levels, Atmos. Environ., 43, 1444–1455, 2009.

Dawson, J. P., Adams, P. J., and Pandis, S. N.: Sensitivity of ozone to summertime climate in the eastern USA: A modeling case study, Atmos. Environ., 41, 1494–1511, 2007.

Dudhia, J.: Numerical study of convection observed during the winter monsoon experiment using a mesoscale two-dimensional model, J. Atmos. Sci., 46, 3077–3107, 1989.

ENVIRON: User's Guide CAMx-Comprehensive Air Quality Model with Extensions, Version 4.30, ENVIRON International Corporation. 415.899.0700, 2006.

Foley, K. M., Roselle, S. J., Appel, K. W., Bhave, P. V., Pleim, J. E., Otte, T. L., Mathur, R., Sarwar, G., Young, J. O., Gilliam, R. C., Nolte, C. G., Kelly, J. T., Gilliland, A. B., and Bash, J. O.: Incremental testing of the Community Multiscale Air Quality (CMAQ) modeling system version 4.7, Geosci. Model Dev., 3, 205–226, doi:10.5194/gmd-3-205-2010, 2010.

Gerasopoulos, E., Kouvarakis, G., Vrekoussis, M., Kanakidou, M., and Mihalopoulos, M.: Ozone variability in the marine boundary layer of the eastern Mediterranean based on 7-year observations, J. Geophys. Res., 110, D15309, doi:10.1029/2005JD005991, 2005.

Gerasopoulos, E., Kouvarakis, G., Babasakalis, P., Vrekoussis, M., Putaud, J.-P., and Mihalopoulos, N.: Origin and variability of particulate matter (PM10) mass concentrations over the Eastern Mediterranean, Atmos. Environ., 40, 4679–4690, 2006a.

Gerasopoulos, E., Kouvarakis, G., Vrekoussis, M., Donoussis, C., Mihalopoulos, N., and Kanakidou, M.: Photochemical ozone production in the Eastern Mediterranean, Atmos. Environ., 40, 3057–3069, 2006b.

Gonçalves, M., Jiménez-Guerrero, P., and Baldasano, J. M.: Contribution of atmospheric processes affecting the dynamics of air pollution in South-Western Europe during a typical summer-time photochemical episode, Atmos. Chem. Phys., 9, 849–864, doi:10.5194/acp-9-849-2009, 2009.

Gong, S. L.: A parameterization of sea-salt aerosol source function for sub- and super-micron particles, J. Geophys. Res., 17, 1097, doi:10.1029/2003GB002079, 2003.

Grell, G. A., Peckham, S. E., Schmitz, R., McKeen, S. A., Frost, G., Skamarock, W. C., and Eder, B.: Fully coupled "online" chemistry within the WRF model, Atmos. Environ., 39, 6957–6975, 2005.

Guenther, A., Karl, T., Harley, P., Wiedinmyer, C., Palmer, P. I., and Geron, C.: Estimates of global terrestrial isoprene emissions using MEGAN (Model of Emissions of Gases and Aerosols from Nature), Atmos. Chem. Phys., 6, 3181–3210, doi:10.5194/acp-6-3181-2006, 2006.

Hogrefe, C., Rao, S. T., Kasibhatla, P., Kallos, G., Tremback, C. J., Hao, W., Olerud, D., Xiu, A., McHenry, J., and Alapaty, K.: Evaluating the performance of regional-scale photochemical modeling systems: Part I-meteorological predictions, Atmos. Environ., 35, 4159–4174, 2001.

Hogrefe, C., Lynn, B., Rosenzweig, C., Goldberg, R., Civerolo, K., Ku, J.-Y., Rosenthal, J., Knowlton, K., and Kinney, P. L.: Utilizing CMAQ process analysis to understand the impacts of climate change on ozone and particulate matter, in: 4th Annual CMAS Models-3 Users' Conference, 26–28 September 2005, Chapel Hill, NC, USA, 2005.

Hong, S.-Y. and Lim, J.-O.: The WRF Single-Moment 6-Class Microphysics Scheme (WSM6), J. Korean Meteor. Soc. 42, 129–151, 2006.

Hong, S.-Y., Dudhia, J., and Chen, S.-H.: A revised approach to ice microphysical processes for the bulk parameterization of clouds and precipitation, Mon. Weather Rev., 132, 103–120, 2004.

Im, U.: Mesoscale modeling of aerosol levels in Istanbul using a high resolution MM5/CMAQ air quality modeling system, PhD Thesis, Bogazici University, Istanbul, Turkey, 2009.

Im, U., Markakis, K., Unal, A., Kindap, T., Poupkou, A., Incecik, S., Yenigun, O., Melas, D., Theodosi, C., and Mihalopoulos, N.: Study of a winter PM episode in Istanbul using high resolution WRF/CMAQ modeling system, Atmos. Environ., 44, 3085–3094, 2010.

Im, U., Poupkou, A., Incecik, S., Markakis, K., Kindap, T., Unal, A., Melas, D., Yenigun, O., Topcu, S., Odman, M.T., Tayanc, M., and Guler, M.: The impact of anthropogenic and biogenic emissions on surface ozone concentrations in Istanbul, Sci. Total Environ., 409, 1255–1265, 2011.

IPCC: Climate change 2007: Synthesis report, Intergovermental Panel on Climate Change, 2007.

Jacob, D. J. and Winner, D. A.: Effect of climate change on air quality, Atmos. Environ., 41, 51–63, 2009.

Kain, J. S.: The Kain-Fritsch convective parameterization: An update, J. Appl. Meteorol., 43, 170–181, 2004.

Kallos, G., Astitha,, M., Katsafados, P., and Spyrou, Ch.: Long-range transport of anthropogenically and naturally produced particulate matter in the Mediterranean and North Atlantic: Current state of knowledge, J. Appl. Meteorol. Climatol., 46, 1230–1251, 2007.

Kanakidou, M., Mihalopoulos, N., Kalivitis, N., Tsigaridis, K., Kouvarakis, G., Koulouri, E., Gerasopoulos, E., Vrekoussis, M., and Myriokefalitakis, S.: Natural contributions to particulate matter levels over Europe – the experience from Greece, International Conference on Science and Technology (CEST) 2007, A-585-592, 2007.

Kanakidou, M., Mihalopoulos, N., Kindap, T., Im, U., Vrekoussis, M., Gerasopoulos, E., Dermitzaki, E., Unal, A., Kocak, M., Markakis, K., Melas, D., Kouvarakis, G., Youssef, A. F., Richter, A., Hatzianastassiou, N., Hilboll, A., Ebojie, F., von Savigny, C., Ladstaetter-Weissenmayer, A., Burrows, J., and Moubasher, H.: Megacities as hot spots of air pollution in the East Mediterranean, Atmos. Environ., 45, 1223–1235, 2011.

Kindap, T., Unal, A., Chen, S. H., Hu, Y., Odman, M. T., and Karaca, M.: Long-range aerosol transport from Europe to Istanbul, Turkey, Atmos. Environ., 40, 3536–3547, 2006.

Lazaridis, M., Spyridaki, A., Solberg, S., Smolk, J., Zdímal, V., Eleftheriadis, K., Aleksanropoulou, V., Hov, O., and Georgopoulos, P. G.: Mesoscale modeling of combined aerosol and photooxidant processes in the Eastern Mediterranean, Atmos. Chem. Phys., 5, 927–940, doi:10.5194/acp-5-927-2005, 2005.

Lelieveld, J., Berresheim, H., Borrmann, S., Crutzen, P. J., Dentener, F. J., Fischer, H., Feichter, J., Flatau, P. J., Heland, J., Holzinger, R., Korrmann, R., Lawrance, M. G., Levin, Z., Markowiz, K. M., Mihalopoulos, N., Minikin, A., Ramanathan, V., de Reus, M., Roelofs, G. J., Scheeren, H. A., Sciare, J., Schlager, H., Schultz, M., Siegmund, P., Steil, B., Stephanou, E. G., Stier, P., Traub, M., Warneke, C., Williams, J., and Ziereis, H.: Global air pollution crossroads over the Mediterranean, Science, 298, 794–799, 2002.

Liakakou, E., Vrekoussis, M., Bonsang, B., Donousis, C., Kanakidou, M., and Mihalopoulos, N.: Isoprene above the Eastern Mediterranean: Seasonal variation and contribution to the oxidant capacity of the atmosphere, Atmos. Environ., 41, 1002–1010, 2007.

Liao, K.-J., Tagaris, E., Manomaiphiboon, K., Wang, C., Woo, J.-H., Amar, P., He, S., and Russell, A. G.: Quantification of the impact of climate uncertainty on regional air quality, Atmos. Chem. Phys., 9, 865–878, doi:10.5194/acp-9-865-2009, 2009.

Markakis, K., Poupkou, A., and Melas, D., Tzoumaka., P., and Petrakakis, M.: A computational approach based on GIS technology for the development of an anthropogenic emission inventory of gaseous pollutants in Greece, Water Air Soil Poll., 207, 157–180, 2010a.

Markakis, K., Poupkou, A., and Melas, D., and Zerefos, C.: A GIS based anthropogenic PM$_{10}$ emission inventory for Greece, Atmos. Poll. Res., 1(2), 71–81, 2010b.

Melas, D., Ziomas, I., Klemm, O., and Zerefos, C.: Anatomy of sea breeze circulation in Greater Athens under weak large-scale ambient winds, Atmos. Environ., 32, 2223–2237, 1998a.

Melas, D., Ziomas, I., Klemm, O., and Zerefos, C.: Flow dynamics in Athens area under moderate large-scale winds, Atmos. Environ., 32, 2209–2222, 1998b.

Melas, D., Kioutsioukis, I., and Lazaridis, M.: The impact of sea breeze on air quality in Athens, Advances in Air Pollution Modeling for Environmental Security. NATO Science Series: IV: Earth and Environmental Sciences, 54, 285–295, 2005.

Mihalopoulos, N., Stephanou, E., Kanakidou, M., Pilitsidis, S., and Bousquet, P.: Tropospheric aerosol ionic composition above the Eastern Mediterranean Area, Tellus B, 314–326, 1997.

Mlawer, E. J., Taubman, S. J., Brown, P. D., Iacono, M. J., and Clough, S. A.: Radiative transfer for inhomogeneous atmospheres: RRTM, a validated correlated-k model for the longwave, J. Geophys. Res., 102, 16663–16682, 1997.

Myriokefalitakis, S., Vrekoussis, M., Tsigaridis, K., Wittrock, F., Richter, A., Brühl, C., Volkamer, R., Burrows, J. P., and Kanakidou, M.: The influence of natural and anthropogenic secondary sources on the glyoxal global distribution, Atmos. Chem. Phys., 8, 4965–4981, doi:10.5194/acp-8-4965-2008, 2008.

Myriokefalitakis, S., Vignati, E., Tsigaridis, K., Papadimas, C., Sciare, J., Mihalopoulos, N., Facchini, M.C., Rinaldi, M., Dentener, F. J., Ceburnis, D., Hatzianastasiou, N., ODowd, C., van Meele, M., and Kanakidou, M.: Global modeling of the oceanic source of organic aerosols, Adv. Meteorol., 939171, 16 pp., doi:10.1155/2010/939171, 2010.

Myriokefalitakis, S., Tsigaridis, K., Mihalopoulos, N., Sciare, J., Nenes, A., Segers, A., and Kanakidou, M.: In-cloud oxalate formation in the global troposphere: a 3-D modeling study, Atmos. Chem. Phys. Discuss., 11, 485–530, doi:10.5194/acpd-11-485-2011, 2011.

Odman, M. T., Hu, Y., Unal, A., Russell, A. G., and Boylan, J. W.: Determining the sources of regional haze in the Southeastern US using the CMAQ model, J. Appl. Meteorol. Climatol., 46(11), 1731–1743, 2007.

Otte, T. L. and Pleim, J. E.: The Meteorology-Chemistry Interface Processor (MCIP) for the CMAQ modeling system: updates through MCIPv3.4.1, Geosci. Model Dev., 3, 243–256, doi:10.5194/gmd-3-243-2010, 2010.

Pleim, J. E.: A combined local and nonlocal closure model for the atmospheric boundary layer. Part I: Model description and testing, J. Appl. Meteorol. Climatol., 46(9), 1383–1395, 2007.

Poupkou, A.: Study of the photochemical air pollution over the Southeastern Europe, PhD thesis of the Aristotle University of Thessaloniki, Thessaloniki, Greece, 2006.

Poupkou, A., Symeonidis, P., Lisaridis, I., Melas, D., Ziomas, I., Yay, O.D. and Balis D.: Effects of anthropogenic emission sources on maximum ozone concentrations over Greece, Atmos. Res., 89, 374–381, 2008.

Poupkou, A., Melas, D., Ziomas, I., Symeonidis, P., Lizaridis, I., Gerasopoulos, E., and Zerefos, C.: Simulated summertime regional ground-level ozone concentrations over Greece, Water Air Soil Poll., 196, 169–181, 2009.

Poupkou, A., Giannaros, T., Markakis, K., Kioutsioukis, I., Curci, G., Melas, D., and Zerefos, C.: A model for European biogenic volatile organic compound emissions: Software development and first validation, Environ. Modell. Softw., 25, 12, 1845–1856, 2010.

Qian, Y., W. I. Gustafson Jr., and Fast, J. D.: Quantifying the subgrid variability of trace gases and aerosols based on WRF-Chem simulations, Atmos. Chem. Phys. Discuss., 10, 10777–10837, doi:10.5194/acpd-10-10777-2010, 2010.

San Jose, R., Perez, J. L., Pleguezuelos, C., Camacho, F., and Gonzalez, R. M.: MM5-CMAQ air quality modeling process analysis: Madrid case, Air pollution X, Ecology and the Environment vol. 53, C. A. BREBBIA, Wessex Institute of Technology, UK and University of the West of England, Bristol, UK, 2002.

Sanchez-Ccoyllo, O., Ynoue, R. Y., Martins, L. D., and Andrade, M. F.: Impacts of ozone precursor limitation and meteorological variables on ozone concentration in Sao Paulo, Brazil, Atmos. Environ., 40, 552–562, 2006.

Seinfeld, J. H. and Pandis, S.: Atmospheric Chemistry and Physics: From Air Pollution to Climate Change, John Wiley & Sons, Inc., New York, 1998.

Sillman, S. and Samson, P. J.: Impact of temperature on oxidant photochemistry in urban, polluted rural and remote environments, J. Geophys. Res., 100(D6), 497–508, 1995.

Simpson, D., Winiwarter, W., Börjesson, G., Cinderby, S., Ferreiro, A., Guenther, A., Hewitt, N., Janson, R., Khalil, M. A. K., Owen, S., Pierce, T. E., Puxbaum, H., Shearer, M., Skiba, U., Steinbrecher, R., Tarrassón, L., and Öquist, M.G.: Inventorying emissions from nature in Europe, J. Geophys. Res., 104, 8113–8152, 1999.

Simpson, D., Fagerli, H., Jonson, J. E., Tsyro, S., Wind, P., and Tuovinen, J.-P.: Transboundary acidification, eutrophication and ground level ozone in Europe. PART I. Unified EMEP model description. EMEP Report 1/2003, Norwegian Meteorological Institute, ISSN 0806-4520, 104 pp., 2003.

Skamarock, W. C. and Klemp, J. B.: A time-split non-hydrostatic atmospheric model, J. Comput. Phys., 227, 3465–3485, 2008.

Smiatek, G. and Steinbrecher, R.: Temporal and spatial variation of forest VOC emissions in Germany in the decade 1994–2003, Atmos. Environ., 40, 166–177, 2006.

Steinbrecher, R., Smiatek, G., Köble, R., Seufert, G., Theloke, J., Hauff, K., Ciccioli, P., Vautard, R., and Curci, G.: Intra- and inter-annual variability of VOC emissions from natural and semi-natural vegetation in Europe and neighboring countries, Atmos. Environ., 43, 1380–1391, 2009.

Symeonidis, P., Poupkou, A., Gkantou, A., Melas, D., Yay, O.D., Pouspourika, E., and Balis, D.: Development of a computational system for estimating biogenic NMVOCs emissions based on GIS technology, Atmos. Environ., 42, 1777–1789, 2008.

Tsigaridis, K., Lathire, J., Kanakidou, M., and Hauglustaine, D. A.: Naturally driven variability in the global secondary organic aerosol over a decade, Atmos. Chem. Phys., 5, 1891–1904, doi:10.5194/acp-5-1891-2005, 2005.

Unal, A., Hu, Y., Chang, M. E., Odman, M. T., Russel, A. G.: Airport related emissions and impacts on air quality: application to the Atlanta International Airport. Atmos. Environ. 39, 5787–5798, 2005.

van Noije, T. P. C., van Eskes, H. J., van Weele, M., and van Velthoven, P. F. J.: Implications of the enhanced Brewer-Dobson circulation in European Centre for Medium-Range Weather Forecasts reanalysis ERA-40 for the stratosphere-troposphere exchange of ozone in global chemistry transport models, J. Geophys. Res. 109, D19308, doi:10.1029/2004JD004586, 2004.

Vrekoussis, M., Mihalopoulos, N., Gerasopoulos, E., Kanakidou, M., Crutzen, P. J., and Lelieveld, J.: Two-years of NO_3 radical observations in the boundary layer over the Eastern Mediterranean, Atmos. Chem. Phys., 7, 315–327, doi:10.5194/acp-7-315-2007, 2007.

Yamartino, R. J.: Nonnegative, conserved scalar transport using grid-cell-centered, spectrally constrained Blackman cubics for applications on a variable-thickness mesh, Mon. Weather Rev., 121, 753–763, 1993.

Yardwood, G., Wilson, G., Emery, C., and Guenther, A.: Development of GLOBEIS-A state of the science biogenic emissions modeling system: Final report, 1999.

Yardwood, G., Rao, S., Yocke, M., and Whitten, G. Z.: Updates to the Carbon Bond chemical mechanism: CB05. Final Report to the US EPA, RT-0400675, 8 December, 2005.

Zhang, K., Knipping, E., Wexler, A., Bhave, P., and Tonnesen, G.: Size distribution of sea-salt emissions as a function of relative humidity, Atmos. Environ., 39, 3373–3379, 2005.

Zhang, Y., Vijayaraghavan, K., Huang, J., and Jacobson, M. Z.: Probing into Regional O_3 and PM Pollution: A 1-year CMAQ Simulation and Process Analysis over the United States, in: 14th Joint Conference on the Applications of Air Pollution Meteorology with the Air and Waste Management Association, 28 Janaury–2 February 2006, Atlanta, GA, USA, 2006.